Università degli Studi di Padova

Dipartimento di Fisica e Astronomia
"Galileo Galilei"

Corso di Laurea in Fisica

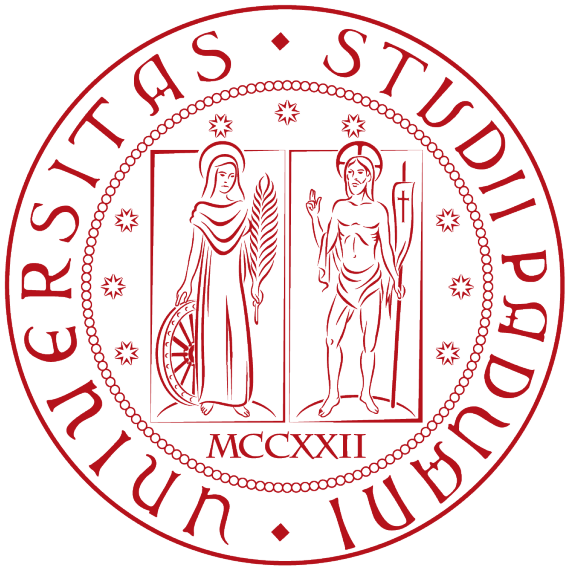

Binary neutron star mergers in the gravitational wave era

Laureando
Griggio Massimo

Relatore
Zendri Jean-Pierre
Correlatore
Ciolfi Riccardo

Anno Accademico 2016/2017

Abstract

After the first direct observations of gravitational waves generated by the coalescence of binary black hole systems, expectations about the possibility to reveal binary neutron star systems are growing. Beyond the chance to probe the "strong" gravity regime and thus the validity of general relativity, these events will allow us to study extreme physical conditions not reproducible on Earth and in particular the behaviour of matter at supranuclear densities. Furthermore, the emission of gravitational waves is accompanied by a wide set of electromagnetic signals which cover the entire spectrum, from gamma to radio, paving the way to a multi-messenger astrophysics. The present work will give a brief overview of these systems, from the formation to the dynamics, with emphasis on the gravitational and electromagnetic emission and on the present and future detection perspectives.

In the first chapter we will introduce neutron stars, starting with a short historical background, and we will report some general information about their structure and present observations. We will give the foundation for a theoretical model of such objects.

In the second chapter we will discuss the formation channels for a binary system and the three phases of binary system coalescence.

In the third chapter we will solve the linearized Einstein field equations, showing that they admit a wave solution. We will then understand how the gravitational wave emission is related to the stress-energy tensor of the source, and we will apply the theory to the case of a binary system.

In the fourth chapter we will give an overview of the most promising electromagnetic counterparts to the gravitational wave signal from binary neutron star mergers.

Contents

List of Figures

List of Tables

1 Neutron stars

1.1 A brief overview

In 1934 Baade and Zwicky [1] proposed the idea of neutron stars (NSs), shortly after the discovery of the neutron by Chadwick [2]. They pointed out that NSs would be at very high density and small radius and much more gravitationally bound than ordinary stars. They also suggested that they would form in supernova collapses. Most of the scientific community ignored Baade and Zwicky proposal for more than 30 years, until 1967, when Bell and Hewish observed [3] with a radio telescope a repeating signal at a fixed declination and right ascension. The signal consisted in a series of pulses equally spaced and always $\sim 1.337\,\mathrm{s}$ apart (Figure 1.1), reason why they are known as "pulsars" (pulsating-stars).

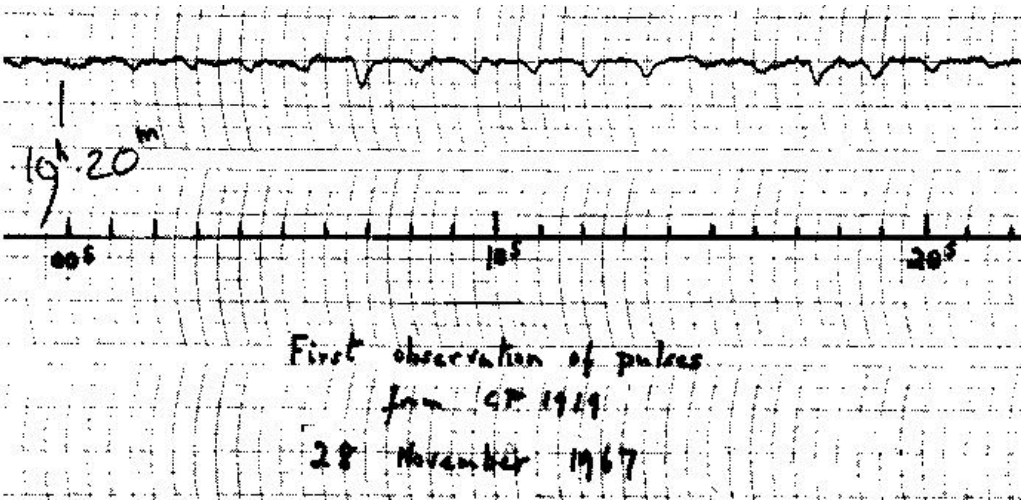

Figure 1.1: The first radio pulsar CP1919 discovered by Hewish and Bell in 1967.[1]

In 1968, Gold and Pacini proposed [4, 5] that these signals are emitted by rotating NSs, and this is generally accepted today. For a star with mass M and radius R, rotating with angular velocity $\omega = \frac{2\pi}{T}$, being T the period, we can find an approximate lower limit for T, requiring that the centrifugal acceleration does not exceed the gravitational acceleration at its equator:

$$\omega^2 R < \frac{GM}{R^2} \tag{1.1.1}$$

[1] https://briankoberlein.com/2014/05/14/little-green-men/

which gives

$$T > \left(\frac{3\pi}{G\rho}\right)^{\frac{1}{2}}, \tag{1.1.2}$$

where $\rho = M\left(\frac{4}{3}\pi R^3\right)^{-1}$ is the mean density. Equation (1.1.2), knowing T, gives a very convervative lower limit for ρ:

$$\rho > \frac{3\pi}{GT^2}. \tag{1.1.3}$$

With data recorded by Hewish and Bell (Figure 1.1), we get $\rho \gtrsim 10^8\,\mathrm{g\,cm^{-1}}$: this density limit is just consistent with the densities of white dwarfs (WDs). But for the faster pulsar soon discovered in the Crab Nebula, with period $T = 0.033\,\mathrm{s}$, we get a density too high for a stable WD. The Crab Nebula is the remnant of a supernova collapse, and this is in agreement with Baade and Zwicky suggestion.

A very simple pulsar model which accounts for many of their observed properties is the oblique rotator magnetic dipole model (Figure 1.2). Radiated energy is given by

$$\dot{E} = -\frac{2}{3c^3}|\ddot{\mathbf{m}}|^2, \tag{1.1.4}$$

with $\mathbf{m}$ being the magnetic dipole associated to the NS. We can write it in terms of the angular velocity ω as

$$\dot{E} = -\frac{B^2R^6\omega^4\sin^2(\alpha)}{6c^3}, \tag{1.1.5}$$

where B is the magnetic field at the surface and α the angle between the magnetic dipole and the rotation axis.

NSs, together with white dwarfs (WDs) and black holes (BHs), belong to a class of astrophysical objects known as compact objects (COs). They differ from normal stars mainly for two reasons: first, they are not supported by thermal pressure due to nuclear fusion. WDs are supported by the degeneration pressure of electrons, while in NSs degeneration pressure is given by neutrons. On the other hand, BHs are fully collapsed objects, in which gravity is so strong that nothing can contrast it and matter collapses to a singularity. Second, they have much smaller radii relative to normal stars with comparable mass, and hence much stronger surface gravitational field.

To determine the structure of NSs we need a general relativistic model for spherically symmetric bodies in static gravitational equilibrium, and an equation of state (EOS) for degenerate matter which relates pressure to density.

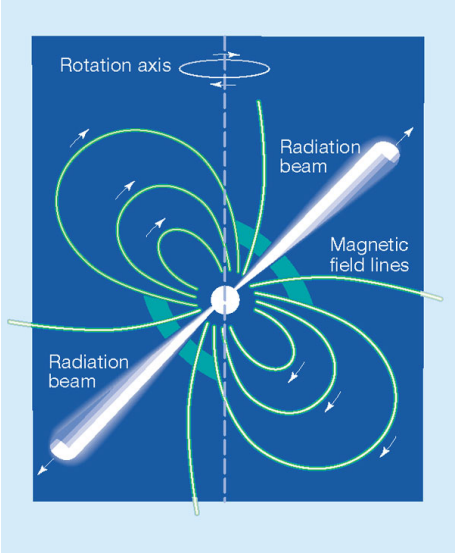

Figure 1.2: Magnetic dipole model for pulsars.[2]

1.2 Neutron stars models

1.2.1 Tolman–Oppenheimer–Volkoff equation

Since the extreme gravitional fields play a crucial role in NSs and their equilibrium configuration, we need general relativity to determine the equations to describe their structure. We follow Tolman-Oppenheimer-Volkoff (TOV) for the general relativistic model of NSs. Starting with Einstein field equations

$$R_{\mu\nu} - \frac{1}{2} g_{\mu\nu} R = \frac{8\pi G}{c^4} T_{\mu\nu}, \tag{1.2.1}$$

and denoting $d\Omega^2 \equiv d\theta^2 + \sin^2\theta d\phi^2$, we take the most general spherically symmetric metric

$$ds^2 = -Adt^2 + Bdr^2 + 2Cdtdr + Dd\Omega^2, \tag{1.2.2}$$

with t, r, θ and ϕ being the time, radial and angular coordinate respectively. Since we are looking for a static solution, A, B, C and D are functions of r only. Equation (1.2.2) can be easily rewritten in a more convenient form. We'll consider the following metric equivalent to (1.2.2):

$$ds^2 = -e^{2\Phi}dt^2 + e^{2\lambda}dr^2 + r^2 d\Omega^2, \tag{1.2.3}$$

[2] https://www.nature.com/nature/journal/v406/n6792/fig_tab/406139a0_ft.html

where Φ and λ are functions of r. To obtain the TOV equation we assume that the stellar material can be treated as a perfect fluid. The stress-energy tensor is then

$$T^{\mu\nu} = \left(\rho + \frac{P}{c^2}\right) u^\mu u^\nu + P g^{\mu\nu}, \tag{1.2.4}$$

where ρ is the mass density of the fluid, P its pressure and u^μ the four-velocity field. We also define a new metric function $m(r)$ by

$$e^{2\lambda} = \left(1 - \frac{2m}{r}\right)^{-1}. \tag{1.2.5}$$

By equations (1.2.1) with the stress-energy tensor given by (1.2.4), we get:

$$\frac{dm}{dr} = 4\pi r^2 \rho, \tag{1.2.6}$$

$$\frac{dP}{dr} = -\frac{\rho m}{r^2}\left(1 + \frac{P}{\rho}\right)\left(1 + \frac{4\pi P r^3}{m}\right)\left(1 - \frac{2m}{r}\right)^{-1}, \tag{1.2.7}$$

where we set c=G=1. Equation (1.2.7) is known as "Tolman-Oppenheimer-Volkoff equation of hydrostatic equilibrium".

We want the interior metric to smoothly match the exterior Schwarzschild metric

$$ds^2 = -\left(1 - \frac{2M}{r}\right) dt^2 + \left(1 - \frac{2M}{r}\right)^{-1} dr^2 + r^2 d\Omega^2, \tag{1.2.8}$$

where M denotes the total mass of the gravitational field's source. The quantity $m(r)$ must then be equal to M at $r = R$, being R the radius of the star, hence the interpretation of $m(r)$ as the total mass inside radius r. From (1.2.6) we get the following expression for the total mass of the star:

$$M = \int_0^R 4\pi r^2 \rho dr. \tag{1.2.9}$$

This includes all contributions to the relativistic mass, including gravitational binding energy. Equations (1.2.6) and (1.2.7), together with an EOS of the form $P = P(\rho)$, lend themselves to easy numerical computation of a general relativistic stellar model by following these steps:

- Pick a value of central density ρ_c and the boundary condition $m(0) = 0$. EOS gives a value for P_c.
- Integrate (1.2.6) and (1.2.7) out from $r = 0$, using the values in the previous step as initial condition. For every obtained value of P, the EOS gives a value for ρ.
- The value $r = R$ at which $P = 0$ is the radius of the star, and $m(R) = M$ the total mass.

Repeating this procedure for different ρ_c, we can obtain different stellar models with varying central densities.

1.2.2 Equations of state

To determine the internal structure of a NS, as we pointed out previously, we need an EOS which links the microscopic information of the system to the macroscopic thermodynamic variables. For densities $\rho < \rho_d = 4 \times 10^{11}\,\mathrm{g/cm^3}$, the properties of matter can be obtained directly from experiments. As ρ increases, inverse β-decay becomes more efficient, and neutrons are produced in large number, while the associated neutrinos leave the star. When ρ reaches ρ_d, there are no more free energy levels available for the neutrons, that must then drip out from the nuclei, forming a neutron gas. This process is called neutron drip. For densities $\rho_d < \rho < \rho_0 = 2.67 \times 10^{14}\,\mathrm{g/cm^3}$, models of the EOS are based on extrapolations of the available empirical data, as the extremely neutron rich nuclei are not observed on Earth.

However, no data is available for matter above the nuclear density ρ_0. EOS models for supranuclear densities are obtained mainly by two approaches: non-relativistic many-body theory (NMBT) and relativistic mean-field theory (RMFT). In NMBT nucleons are considered as point-like particles, whose dynamic is described by the non-relativistic Hamiltonian

$$H = \sum_i \frac{p_i^2}{2m_i} + \sum_{j>i} v_{ij} + \sum_{k>j>i} V_{ijk}, \tag{1.2.10}$$

where the terms v_{ij} and V_{ijk} describe two- and three-nucleons interactions. The resulting problem can be solved exactly.

In RMFT, based on the relativistic quantum field theory, nucleons are described as Dirac particles interacting through meson exchange. In the simplest implementation of this approach, the dynamic is modelled in terms of a scalar field and a vector field. Unfortunately this approach leads to equations of motion which can be solved only in the mean-field approximation, which is known to fail in strongly correlated systems. Employing different EOSs in the TOV equation we get different models for the interior structure of the NS. Several general features emerge, in particular:

- Stars calculated with a stiff EOS have a greater maximum masses than stars derived from a soft EOS.
- Stars derived from a stiff EOS have a lower central density, a larger radius and a much thicker crust than stars of the same mass computed from a soft EOS.

The internal structure of NSs is not well determined, because of uncertainties in the EOS for supranuclear densities. However, we can compute some models based on realistic EOSs.

In Figure 1.3 we show the internal structure computed with two different EOS. The layering is consequence of the onset of different regimes in the EOS as one proceeds to higher densities. We can identify the layers for the stiff EOS as follows:

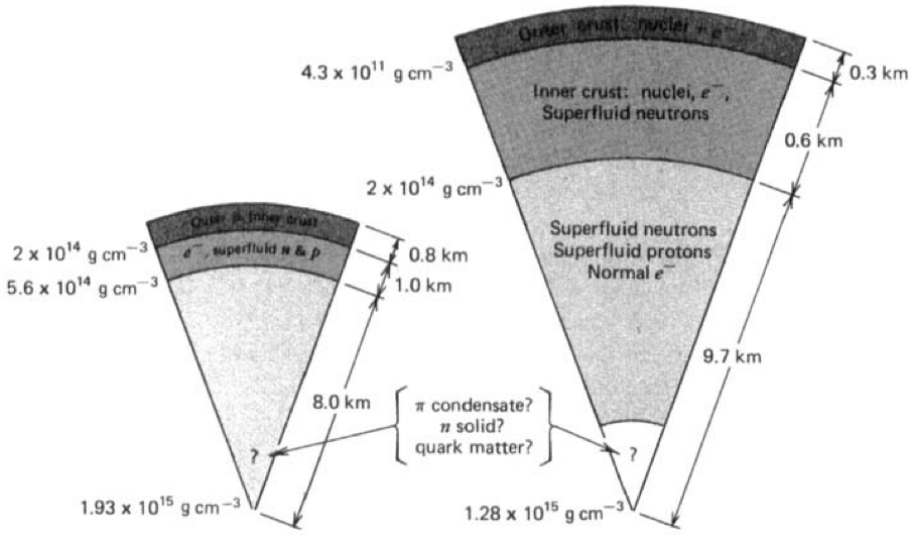

Figure 1.3: Neutron star structure computed with a soft (left) and a stiff (right) equation of state. [6]

- The *surface*, with density $\rho \lesssim 10^6\,\mathrm{g/cm^3}$. In this region the temperatures and the strong magnetic fields can significantly affect the EOS.
- The *outer crust*, with $10^6\,\mathrm{g/cm^3} \lesssim \rho \lesssim \rho_d$. This is a solid region where a lattice of heavy nuclei coexists in β-equilibrium with a degenerate electron gas.
- The *inner crust*, with $\rho_d \lesssim \rho \lesssim \rho_0$. This layer consists of a lattice of neutron-rich nuclei together with a neutron gas and an electron gas.
- The *neutron liquid*, with $\rho_0 \lesssim \rho \lesssim \rho_{core}$. Being this region far above the neutron drip density, it contains mainly free neutrons, with a smaller concentration of protons and normal electrons.
- The *core*, a region where $\rho = \rho_{core} \sim 10^{15}\,\mathrm{g/cm^3}$.

What lies in the core is still an open question. At very high densities, above $10^{15}\,\mathrm{g/cm^3}$, nucleons interactions must be treated relativistically, but relativistic many-body theory for strongly interacting matter is not fully developed. Since at those densities nuclei begin to "touch", one might speculate that matter undergoes a phase transition, at which quarks begin to drip out of the nucleons. This would result in deconfined quark matter. Collins and Perry (1975) suggested that quark matter, for sufficiently high densities, may be treated by first approximation as an ideal, relativistic Fermi gas. However, the existence of stable quark stars is still an unresolved issue.

Since observational properties of a NS depend on the EOS, observations can shed light on the properties of matter at supranuclear density. This is the main reason why NSs are often said to represent *ideal laboratories to study physics under extreme conditions that cannot be reproduced on earth.*

1.2.3 Neutron star masses and radii

By measuring the mass of a NS we can infer information about the stellar evolution of its progenitor, the composition and the EOS, and test general relativity in the strong gravity regime. If the NS is in a binary system we can determine its mass by measuring the six Keplerian parameters and the five post-Keplerian parameters (needed when general relativistic effects are important). The post-Keplerian parameters are measured by radio pulsar timing techniques and rely on the measurement of relativistic effects in the binary orbit. Observational data are shown in Figure 1.4. Concerning the radii of a NS, we can obtain an upper and a lower limit from

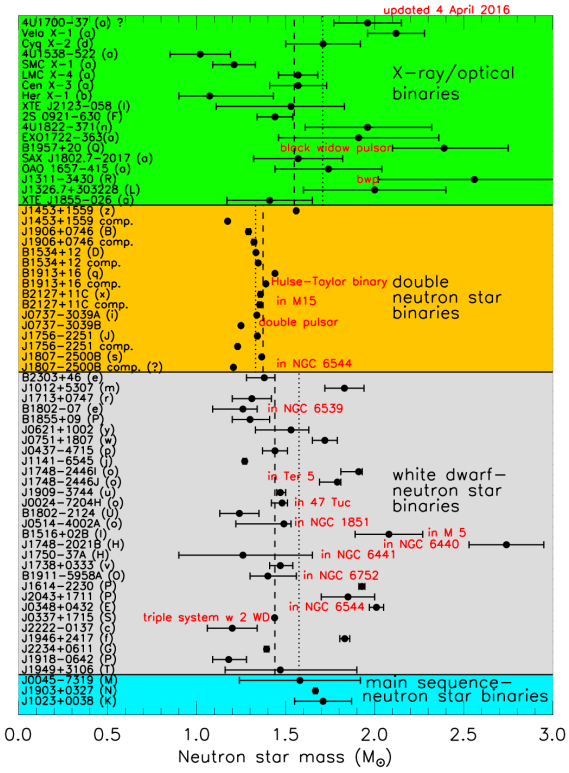

Figure 1.4: Measured masses of neutron stars.[3]

[3] J. Lattimer, Annual Review of Nuclear and Particle Science, Vol. 62, 485, 2012. https://stellarcollapse.org/nsmasses (Jun 2017)

equilibrium relations. Assuming the sound speed has to be lower than the speed of light to preserve causality, and a soft transition between high and low density regions, we find for the lower limit

$$R_{min} \simeq \frac{3GM}{c^2} = 6.2\,\mathrm{km}\left(\frac{M}{1.4M_\odot}\right), \tag{1.2.11}$$

while for the upper limit, including the contribution of the centrifugal force due to the rotational motion

$$R_{max} \simeq \left(\frac{GMP^2}{4\pi^2}\right)^{\frac{1}{3}} = 16.8\,\mathrm{km}\left(\frac{M}{1.4M_\odot}\right)\left(\frac{P}{1\,\mathrm{ms}}\right)^{\frac{2}{3}}, \tag{1.2.12}$$

where with $M_\odot$ we refer to the solar mass. A way to measure NSs' radii is the observation of thermal emission from the NS surface at optical and X-ray frequencies [7].

2 Binary neutron star systems

About half of all stars belong to a binary or multiple stellar system. A binary system consists in a pair of objects orbiting around their centre of mass. If almost one of the two object is a CO it is called a compact binary system. We are interested in those systems composed by two NSs.

2.1 Binary formation channels

Stellar evolution model expect different fates for a star for different values of its initial mass:

- For masses $M < M_\odot$ the star will end its life as a white dwarf.
- For masses $M \gtrsim 8M_\odot$ the star will undergo a supernova explosion. There are then two cases: if $M \lesssim 25M_\odot$ the remnant will be a NS. If $M \gtrsim 25M_\odot$ a BH will form.

We describe the standard formation channel for a binary NS-NS system, illustrated in Figure 2.1. In this scenario there is a massive binary system in which both stars have masses between $\sim (8-25)\, M_\odot$ (to ensure a pair of supernovae). The heavier one evolves over and passes through its giant phase, and finally undergoes a Type Ib, Ic or II supernova, leaving behind what will become the NS. Supposing that the system is not destroyed by the explosion, the companion evolves in turn, reaching the giant phase and overflowing its Roche lobe. The first NS starts accreting matter from the companion and later a common envelope phase can be established, if the mass is transferred too fast to be accreted. Dynamical friction dramatically shrinks the binary separation, until sufficient energy is released to expel the envelope. Without this step the separation would be too wide to lead to a merger within a Hubble time. The core of the secondary will eventually undergo a supernova too, either unbinding the system or leaving a tight binary. While this scenario has been well studied there are several aspects which remain uncertain. In particular:

- The common envelope efficiency, which gives information about the expected range of the binary separation and the mass of the heavier CO after the accretion phase, is poorly constrained.
- The maximum allowed NS mass will affect whether the primary reamains a NS or undergoes accretion-induced collapse to a BH. This value depends upon the nuclear matter EOS, which is not yet determined. The strongest limit is by now set by the binary pulsar PSR J1614-2230, for which a mass of

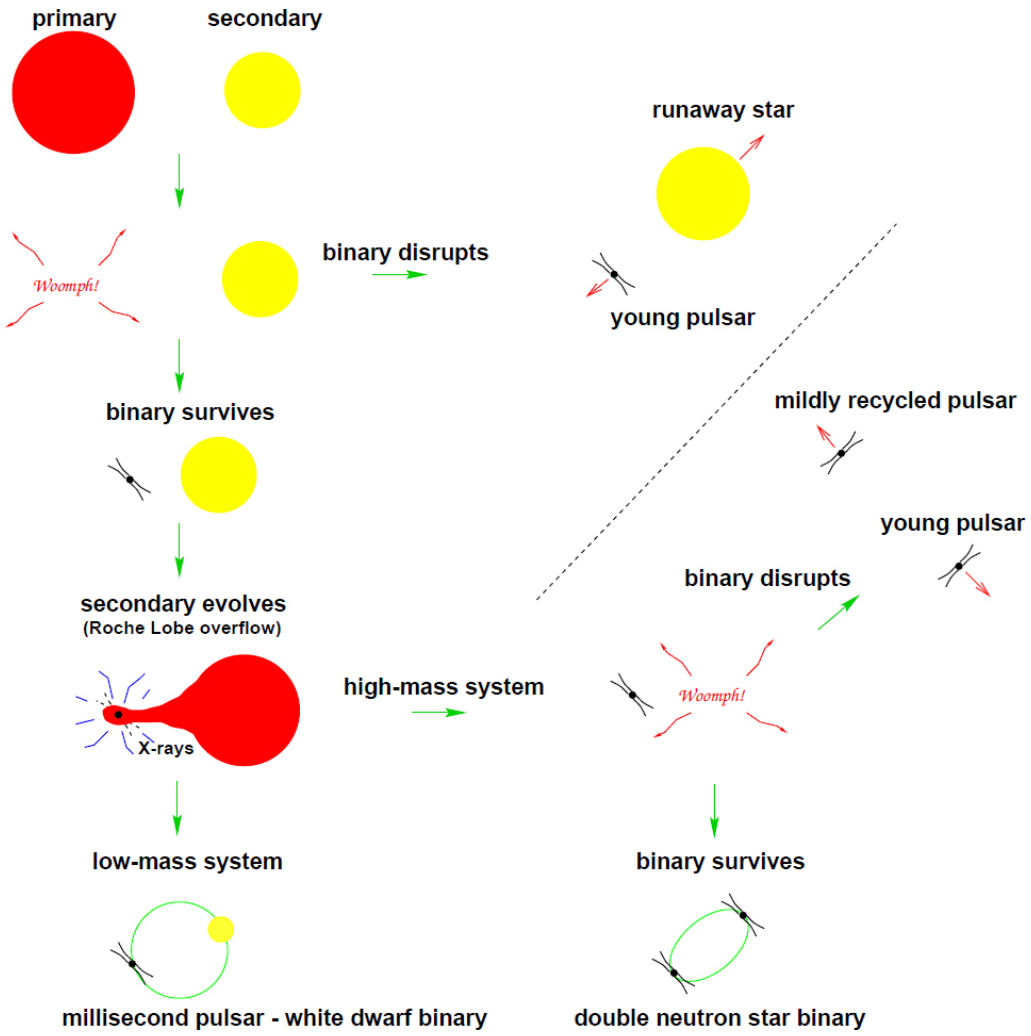

Figure 2.1: Standard formation channels for close NS-NS binaries. [8]

$M = 1.97 \pm 0.04 M_\odot$ was determined by Shapiro time delay measurements [9] (see also [10]).

- The supernova kick velocity distribution is only partially understood, so we can't predict if the system will become unbound after the explosion.

2.2 Stages of a binary merger

The compact binary system evolution can be divided in three phases: inspiral, merger and ringdown. In Figure 2.2 we show an illustration of the three phases with the associated gravitational wave signal expected.

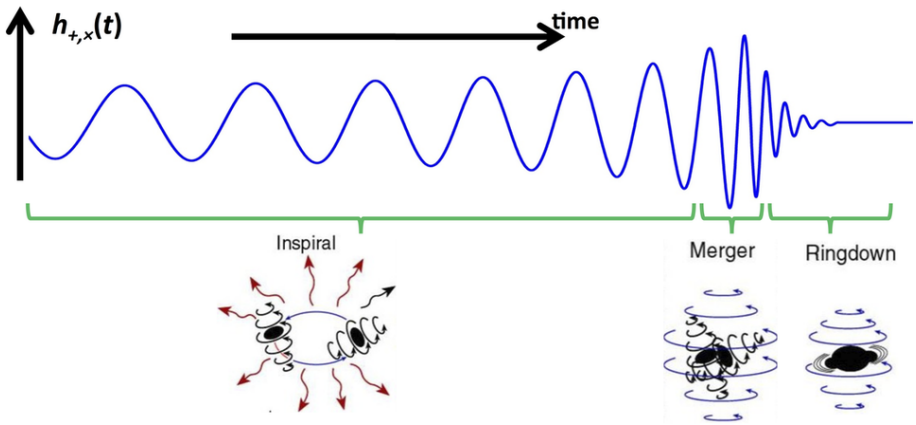

Figure 2.2: Illustration of the merger phases with the gravitational wave signal associated.[1]

Inspiral During the inspiral phase the two objects orbit around their centre of mass. Their orbit shrinks gradually, reducing their distance, due to gravitational wave emission (see Chapter 3). The first stage of the inspiral phase takes a long time, because the gravitational radiation emitted has very low power. In this phase we can threat the two COs as point-like masses, and calculate the power emission by gravitational radiation in the Newtonian approximation. We will do it in Section 3.4, after we have introduced gravitational waves.

Merger The merger phase begins when the two objects come into contact. The Newtonian approximation is no longer valid here, as the system is governed by strong gravitational field and involves tidal deformation and disruption, so we can not consider the masses as point-like. To understand the dynamics in this phase we need full general relativistic simulations, which are also predicting the gravitational wave emission. The merger of two NSs is not well understood principally due to the uncertainty about the EOS and the effect of the magnetic fields. Gravitational waves produced during this stage carry important information about the structure of the NS and thus about the EOS for supranuclear density. This phase takes very short time: from milliseconds to seconds, depending on the masses.

Ringdown After the merger phase the emitted radiation can be computed by perturbation theory. It consists of a superposition of quasi-normal modes of the remnant, which can give information about the object: in case of a BH remnant, the quasi-normal modes depend on the mass and angular momentum. For a NS remnant instead there is a relation with the EOS. The remaining object will "ring", namely will be oscillating in shape around an equilibrium, emitting gravitational

[1] http://www.soundsofspacetime.org/coalescing-binaries.html

waves due the oscillation asymmetry. The oscillating modes are quasi-normal, being damped by the gravitational waves emission. Signals in this stage are emitted in a very short time, varying from milliseconds to seconds as the previous phase, depending again on the mass of the remnant.

Unlike the BH-BH mergers (recently observed by LIGO [11]), which are not expected to produce bright electromagnetic counterparts to their gravitational wave signal, NS-NS mergers are expected to (as we will see in Chapter 4), and observing these two kind of signals together offers a unique opportunity to constrain the EOS of matter at supranuclear densities. Moreover, NS-NS mergers are also a prime candidate astrophysical site for the production of heavy elements in the Universe, via r-process nucleosynthesis in the matter ejected during, and possibly after, the merger.

2.3 Post-merger scenarios

While NS-BH (and obviously BH-BH) mergers will unavoidably end up in a BH, possibly surrounded by a massive accretion disk, after a NS-NS merger there are three different possibility for the remnant to be, depending on the EOS and the masses (Figure 2.3):

- a BH will form. It is still possible.
- The binary NS will merge into a hypermassive NS (HMNS), a NS with mass above the maximum mass allowed for uniformly rotating configurations. Typically, HMNSs will collapse into a BH on a timescale of $\sim$ ms. Common believe is that HMNSs are supported by the rapid rotation of the core, and undergo a collapse when enough differential rotation is carried away by gravitational radiation emission or electromagnetic torque.
- The binaries will merge into a long-lived NS, which we assume to be either supramassive (SMNS, a NS with mass above the maximum allowed for non rotating configurations) or indefinitely stable. SMNSs can survive for minutes or even longer, against the ms of the HMNS. They are believed to be supported by uniform rotation and to collapse when enough angular momentum is removed via magnetic dipole radiation.

However, the mechanism leading to the collapse to a BH of HMNSs and SMNSs is still poorly understood, since a growing number of simulations indicate that they both have slowly rotating cores and that collapse is avoided because a significant amount of matter in the outer layers approaches Kepler velocity. [13, 14, 15]

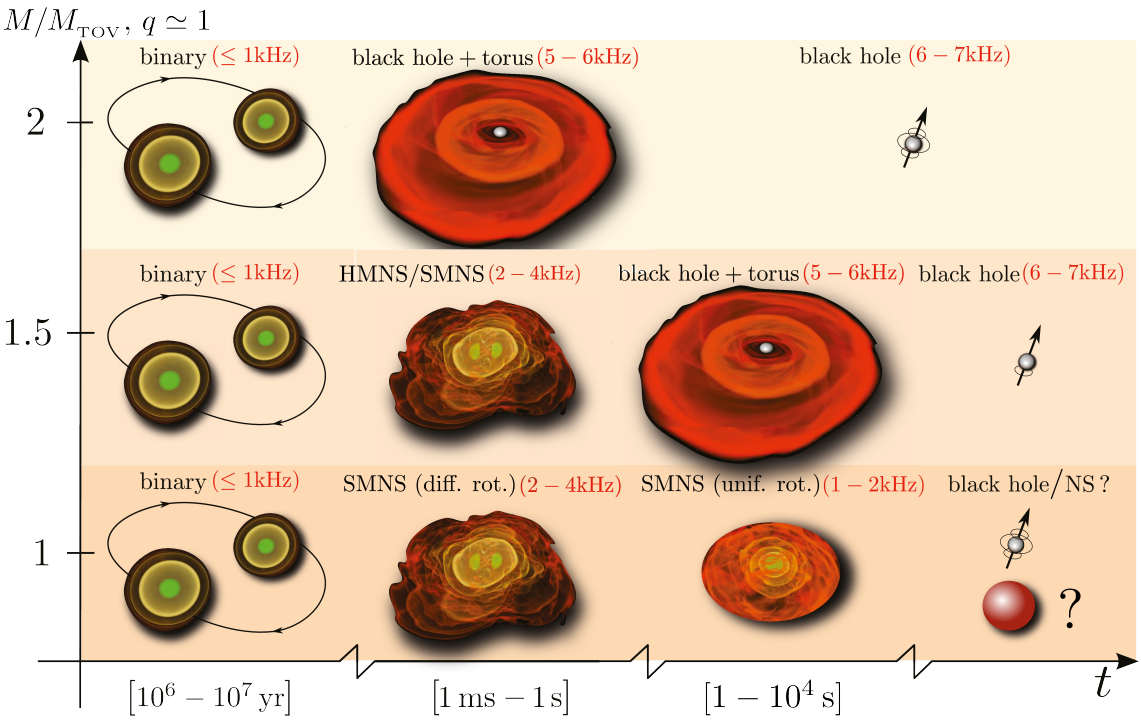

Figure 2.3: Post-merger scenarios for NS-NS coalescences. [12]

Binary NS mergers leading to a NS (hypermassive, supramassive or stable) are characterized by a post-merger phase in which the gravitational waves emission can be significant for several milliseconds and much stronger than those emitted by a BH remnant ringdown signal. The post-merger signal carries information about the remnant structure, thus representing another promising way to constrain the NS EOS.

3 Gravitational radiation from compact binary systems

In this chapter we discuss the generation of gravitational waves according to general relativity. Sections 3.1, 3.2 and 3.3 are devoted to compute generic gravitational wave solutions and the associated power. In Sections 3.4, 3.4.1 and 3.4.2 we consider the case of a compact binary system during the inspiral phase, the binary evolution due to gravitational radiation, and the resulting signal (the characteristic "chirp"). Finally, in Section 3.5, we briefly discuss the recent discovery of binary black hole mergers by the LIGO-Virgo collaboration, which provides direct examples of gravitational wave signals from compact binary inspirals and mergers.

3.1 Wave solutions to the linearized Einstein field equations

In the weak field limit we can linearize Einstein field equations (1.2.1) by writing the space-time metric as

$$g_{\mu\nu} = \eta_{\mu\nu} + h_{\mu\nu}, \tag{3.1.1}$$

where $\eta_{\mu\nu} = diag\,(-1, +1, +1, +1)$ is the smooth Minkowski metric and $h_{\mu\nu}$ a small perturbation, so that $|h_{\mu\nu}| \ll 1$. In this limit, the Christoffel symbols can be written as

$$\Gamma^{\mu}{}_{\alpha\beta} = \frac{1}{2}\eta^{\mu\nu}\left(\partial_\beta h_{\alpha\nu} + \partial_\alpha h_{\beta\nu} - \partial_\nu h_{\alpha\beta}\right) = \frac{1}{2}\left(\partial_\beta h_{\alpha}{}^{\mu} + \partial_\alpha h_{\beta}{}^{\mu} - \partial^\mu h_{\alpha\beta}\right), \tag{3.1.2}$$

and the Ricci tensor becomes

$$R_{\mu\nu} = \frac{1}{2}\left(\partial_\nu\partial_\alpha h_{\mu}{}^{\alpha} + \partial_\mu\partial_\alpha h_{\nu}{}^{\alpha} - \partial_\alpha\partial^\alpha h_{\mu\nu} - \partial_\mu\partial_\nu h^{\alpha}{}_{\alpha}\right). \tag{3.1.3}$$

Introducing the new symmetric second-rank tensor

$$\bar{h}_{\mu\nu} = h_{\mu\nu} - \frac{1}{2}\eta_{\mu\nu}h^{\alpha}{}_{\alpha}, \tag{3.1.4}$$

and imposing the gauge conditions

$$\partial_\nu \bar{h}^{\mu\nu} = 0, \tag{3.1.5}$$

the field equations are then

$$\Box\bar{h}_{\mu\nu} = -\frac{16\pi G}{c^4}T_{\mu\nu}\,, \tag{3.1.6}$$

in which $\Box = \partial^\mu \partial_\mu$ is the d'Alambert operator. The simplest solution to (3.1.6) in void is the monochromatic, plane-wave solution function

$$\bar{h}_{\mu\nu} = A_{\mu\nu} e^{ik_\alpha x^\alpha} + A_{\mu\nu} e^{-ik_\alpha x^\alpha}, \tag{3.1.7}$$

with $A_{\mu\nu}$ and k_μ satisfying

$$k_\alpha k^\alpha = 0, \tag{3.1.8}$$
$$A_{\mu\alpha} k^\alpha = 0. \tag{3.1.9}$$

This solution clearly describes a wave with frequency $\omega = k^0$, which propagates with the speed of light in the direction $\frac{1}{k^0}(k_1, k_2, k_3)$.

3.2 Generation of gravitational waves

We can solve equations (3.1.6) in analogy with electrodynamics. For the electromagnetic four-potential we have

$$\Box A^\mu = \frac{1}{c} j^\mu, \tag{3.2.1}$$
$$\partial_\mu A^\mu = 0, \tag{3.2.2}$$

which has the same structure of (3.1.5) and (3.1.6). The exact solution is then

$$\bar{h}^{\mu\nu} = G_{ret} * \left(-\frac{16\pi G}{c^4} T^{\mu\nu} \right) = -\frac{4G}{c^4} \int \frac{T^{\mu\nu}\left(t - \frac{|\vec{x}-\vec{y}|}{c}, \vec{y}\right)}{|\vec{x}-\vec{y}|} d^3y \tag{3.2.3}$$

where $G_{ret}(x) = \frac{1}{4\pi r}\delta(t-r)$ is the retarded Green function. Faraway from the source we can approximate $|\vec{x}-\vec{y}|$ with the distance r from the source itself, so

$$\bar{h}^{\mu\nu}(t, \vec{x}) = -\frac{4G}{c^4 r} \int T^{\mu\nu}\left(t_{ret} + \frac{\vec{n}\cdot\vec{y}}{c}, \vec{y} \right) d^3y, \tag{3.2.4}$$

with $\vec{n} = \frac{\vec{x}}{r}$. Equations (3.2.4) relate the deviation from the smooth Minkowski metric in the observer frame $(t, \vec{x})$ to the stress-energy tensor of a source distant r from its origin, evaluated at the retarded time $t_{ret} = t - \frac{r}{c}$. The quantity $\frac{\vec{n}\cdot\vec{y}}{c}$ represents the microscopic retard, which can be ignored if the speed of the source is non relativistic.

3.3 Power emission by gravitational wave radiation

We want to derive a law to describe the power emission of a body which emits gravitational waves. It is easy to demonstrate that $\bar{h}^{\mu\nu}$ from equations (3.2.4) fulfills the relations

$$\partial_\rho \bar{h}^{\mu\nu} = \frac{1}{c^3} n_\rho \dot{\bar{h}}^{\mu\nu} \tag{3.3.1}$$

$$n_\mu \dot{\bar{h}}^{\mu\nu} = 0 \tag{3.3.2}$$

and

$$n_\mu n^\mu = 0, \tag{3.3.3}$$

where we set $n^\mu = (1, \vec{n})$. We need an expression for the stress-energy tensor of the gravitational field itself. Fortunately, in the weak field limit, for a field which follows (3.3.1), (3.3.3) and (3.3.3), the expression we look for is easy:

$$T^{\mu\nu}_{grav} = \frac{c^4}{32\pi G} \left(\partial_\mu \bar{h}^{\alpha\beta} \partial_\nu \bar{h}_{\alpha\beta} - \frac{1}{2} \partial_\mu \bar{h}^\alpha{}_\alpha \partial_\nu \bar{h}^\beta{}_\beta \right). \tag{3.3.4}$$

Again, in analogy with electrodynamics, we can determine the angular power emitted distribution as

$$\frac{dW_{grav}}{d\Omega} = cr^2 \left(T^{0i}_{grav} n^i \right), \tag{3.3.5}$$

and the total power as

$$W_{grav} = \int \frac{dW_{grav}}{d\Omega} d\Omega, \; r \to \infty. \tag{3.3.6}$$

Using (3.3.1), (3.3.2) and (3.3.3), we can write (3.3.4) in the form

$$T^{\mu\nu}_{grav} = \frac{n^\mu n^\nu c^4}{32\pi G} \left(\dot{\bar{h}}^{\alpha\beta} \dot{\bar{h}}_{\alpha\beta} - \frac{1}{2} \left(\dot{\bar{h}}^\alpha{}_\alpha \right)^2 \right), \tag{3.3.7}$$

and, after some steps, we find for the angular power emitted distribution the expression

$$\frac{dW_{grav}}{d\Omega} = \frac{r^2 c^3}{32\pi G} \dot{\bar{h}}^{ij} \dot{\bar{h}}^{lm} \Lambda^{ijlm}, \tag{3.3.8}$$

where $\Lambda^{ijlm} = \delta^{il}\delta^{jm} - \frac{1}{2}\delta^{ij}\delta^{lm} - 2\delta^{il}n^j n^m + \delta^{ij} n^l n^m + \frac{1}{2} n^i n^j n^l n^m$. In the non-relativistic limit we can write the spatial components of $\bar{h}$ as

$$\bar{h}^{ij} = -\frac{4G}{rc^4} \int T^{ij} \left(t - \frac{r}{c}, \vec{y} \right) d^3 y. \tag{3.3.9}$$

Introducing the mass-quadrupole moment of the source

$$Q^{ij} = \frac{1}{c^2}\int y^i y^j T^{00} d^3y, \tag{3.3.10}$$

since

$$\int T^{ij} d^3y = \frac{1}{2}\ddot{Q}^{ij}, \tag{3.3.11}$$

we find that $\bar{h}^{ij}$ is related to Q^{ij} by the relation

$$\bar{h}^{ij}\left(t, \vec{x}\right) = -\frac{2G}{rc^4}\ddot{Q}^{ij}\left(t - \frac{r}{c}\right). \tag{3.3.12}$$

Using (3.3.12) into (3.3.5), we get

$$\frac{dW_{grav}}{d\Omega} = \frac{G}{8\pi c^5}\dddot{Q}^{ij}\dddot{Q}^{lm}\Lambda^{ijlm}, \tag{3.3.13}$$

and, integrating over the solid angle, we finally get an expression for the total power emitted

$$W_{grav} = \frac{G}{5c^5}\dddot{\mathcal{Q}}^{ij}\dddot{\mathcal{Q}}^{ij}, \tag{3.3.14}$$

where $\mathcal{Q}^{ij} = Q^{ij} - \frac{1}{3}\delta^{ij}Q^k{}_k$ is the reduced mass-quadrupole moment.

3.4 Gravitational waves from binary systems

We want to determine the signal emitted by a compact system orbiting around its centre of mass during the inspiral phase. As we anticipated in Section 2.2, we can threat the two objects as point-like masses until the merger. Let

$$l \equiv r_1 + r_2 \tag{3.4.1}$$

be the distance between the objects (see Figure 3.1),

$$M \equiv m_1 + m_2 \tag{3.4.2}$$

the total mass and

$$\mu \equiv \frac{m_1 m_2}{M} \tag{3.4.3}$$

the reduced mass. It is easy to calculate the orbital frequency ω with classical mechanics:

$$\omega = \sqrt{\frac{GM}{l^3}}. \tag{3.4.4}$$

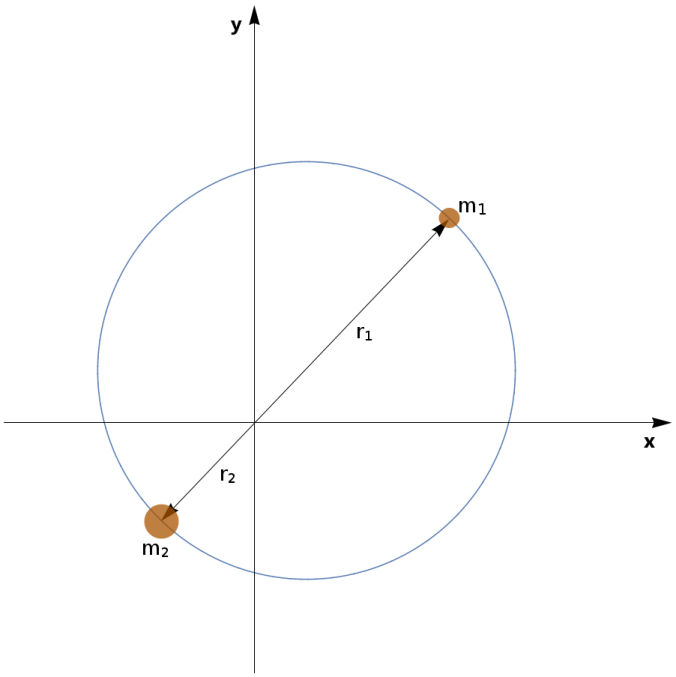

Figure 3.1: Centre of mass frame for binary system. Angular velocity is perpendicular to x and y axes.

On the orbital plane the coordinates for the masses m_1 and m_2 are

$$x_1 = \frac{m_2}{M} l \cos(\omega t), \tag{3.4.5}$$

$$y_1 = \frac{m_2}{M} l \sin(\omega t), \tag{3.4.6}$$

$$z_1 = 0, \tag{3.4.7}$$

$$x_2 = -\frac{m_1}{M} l \cos(\omega t), \tag{3.4.8}$$

$$y_2 = -\frac{m_1}{M} l \sin(\omega t), \tag{3.4.9}$$

$$z_2 = 0. \tag{3.4.10}$$

The 00-component of the stress-energy tensor then is

$$T^{00} = c^2 \sum_{n=1}^{2} m_n \delta(x - x_n) \delta(y - y_n) \delta(z), \tag{3.4.11}$$

and the non-vanishing components of the mass-quadrupole moment (3.3.10) are

$$Q^{11} = \mu l^2 \cos^2(\omega t) = \frac{\mu}{2} l^2 \cos(2\omega t) + cost., \tag{3.4.12}$$

$$Q^{22} = \mu l^2 \sin^2(\omega t) = -\frac{\mu}{2} l^2 \cos(2\omega t) + cost. \tag{3.4.13}$$

and

$$Q^{12} = \mu l^2 \cos(\omega t) \sin(\omega t) = \frac{\mu}{2} l^2 \sin(2\omega t). \tag{3.4.14}$$

From 3.3.12 we find

$$\bar{h}^{ij}(t, \vec{x}) = -\frac{2G}{rc^4} (2\omega)^2 Q^{ij}. \tag{3.4.15}$$

Defining the matrix A^{ij} as

$$A(t) = \begin{bmatrix} \cos(2\omega t) & \sin(2\omega t) & 0 \\ \sin(2\omega t) & -\cos(2\omega t) & 0 \\ 0 & 0 & 0 \end{bmatrix} \tag{3.4.16}$$

we can write Q^{ij} as

$$Q^{ij} = \frac{\mu}{2} l^2 A^{ij}, \tag{3.4.17}$$

and we can rewrite (3.4.15) in the following form:

$$\bar{h}^{ij}(t, \vec{x}) = \frac{2G}{rc^4} \frac{\mu}{2} l^2 (2\omega)^2 A^{ij} \left(t - \frac{r}{c}\right). \tag{3.4.18}$$

Recalling (3.4.4), and defining the wave amplitude

$$h_0 = \frac{4\mu M G^2}{rlc^4} \tag{3.4.19}$$

we finally get

$$\bar{h}^{ij}(t, \vec{x}) = h_0 A^{ij} \left(t - \frac{r}{c}\right). \tag{3.4.20}$$

From these equations we see that the radiation is emitted at twice the orbital frequency.

3.4.1 Power emission

As we found in Section 3.3, the total power is given by (3.3.14), so we need to calculate the time dependent components of the reduced mass-quadrupole moment $\mathcal{Q}^{ij}$. Remembering that

$$\mathcal{Q}^{ij} = Q^{ij} - \frac{1}{3} \delta^{ij} Q^k{}_k, \tag{3.4.21}$$

and noting that Q^{ij} calculated in the previous section is traceless, those components are

$$\mathcal{Q}^{11} = -\mathcal{Q}^{22} = \frac{\mu}{2} l^2 \cos(2\omega t) \tag{3.4.22}$$

and

$$\mathcal{Q}^{12} = \frac{\mu}{2} l^2 \sin(2\omega t). \tag{3.4.23}$$

The power emitted is

$$W_{grav} \equiv \frac{dE_{grav}}{dt} = \frac{32}{5} \frac{G^4}{c^5} \frac{\mu^2 M}{l^5}. \tag{3.4.24}$$

This expression has to be considered as an average over several periods since the gravitational field energy can not be defined locally in general relativity.

We suppose that the system has the time to adjust the orbit to compensate the energy lost by gravitational radiation changing the orbital energy, such that

$$\frac{dE_{orb}}{dt} + W_{grav} = 0. \tag{3.4.25}$$

The orbital energy is given by the sum of the kinetic and potential energy

$$E_{orb} = E_k + V = \frac{1}{2} m_1 \omega^2 r_1^2 + \frac{1}{2} m_2 \omega^2 r_2^2 - \frac{G m_1 m_2}{l} = -\frac{1}{2} \frac{G\mu M}{l}, \tag{3.4.26}$$

and

$$\frac{dE_{orb}}{dt} = -E_{orb} \left(\frac{1}{l} \frac{dl}{dt} \right). \tag{3.4.27}$$

Since $\omega = \frac{2\pi}{T}$, where T is the orbital period, with (3.4.4) we can write (3.4.27) in terms of T as follows

$$\frac{dE_{orb}}{dt} = -\frac{2}{3} \frac{E_{orb}}{T} \frac{dT}{dt}, \tag{3.4.28}$$

and remembering that $\frac{dE_{orb}}{dt} = -W_{grav}$, we finally find how the orbital period changes due to the emission of gravitational waves:

$$\frac{dT}{dt} = \frac{3}{2} \frac{T}{E_{orb}} W_{grav}. \tag{3.4.29}$$

From (3.4.27) we can also find how the separation l changes in time. We get

$$\frac{1}{l} \frac{dl}{dt} = \frac{W_{grav}}{E_{orb}} = -\left(\frac{64}{5} \frac{G^3}{c^5} \mu M^2 \right) \frac{1}{l^4}. \tag{3.4.30}$$

Integrating (3.4.30), assuming that $l(t=0) = l_0$, we obtain

$$l(t)^4 = l_0^4 - \frac{256}{5} \frac{G^3}{c^5} \mu M^2 t, \tag{3.4.31}$$

which can be written as

$$l(t) = l_0 \left(1 - \frac{t}{t_{coal}} \right)^{\frac{1}{4}} \tag{3.4.32}$$

defining $t_{coal} = \frac{5}{256}\frac{c^5}{G^3}\frac{l_0^4}{\mu M^2}$.

From (3.4.32) we see that the separation becomes null when $t = t_{coal}$. Since in fact the masses are not point-like, the merger starts before $t = t_{coal}$. Furthermore, when the two stars are close enough, the weak field approximation and the slow motion assumption are not satisfied, making the quadrupole formalism failing. However, t_{coal} gives an indication of the time that the system needs to merge starting from an orbital distance l.

3.4.2 Emitted waveform

By (3.4.32) we can compute how ω changes in time:

$$\omega(t) = \sqrt{\frac{GM}{l(t)^3}} = \omega_0 \left(1 - \frac{t}{t_{coal}}\right)^{-\frac{3}{8}}, \tag{3.4.33}$$

with $\omega_0 = \sqrt{\frac{GM}{l_0^3}}$. As we previously found, the frequency is twice the orbital period, $\nu_{GW}(t) = 2\frac{\omega(t)}{2\pi}$, and the amplitude is given by (3.4.19):

$$h_0(t) = \frac{4\mu M G^2}{rc^4 l(t)} = \frac{4\pi^{\frac{2}{3}} G^{\frac{5}{3}} \mathcal{M}^{\frac{5}{3}}}{c^4 r} \nu_{GW}(t)^{\frac{2}{3}}, \tag{3.4.34}$$

where $\mathcal{M} = \mu^{\frac{3}{5}} M^{\frac{2}{5}}$ is said *chirp mass*.

Equation (3.4.34) shows that the amplitude and the frequency increase in time, in a way similar to the "chirp" of a bird. An example is shown in Figure 3.2.

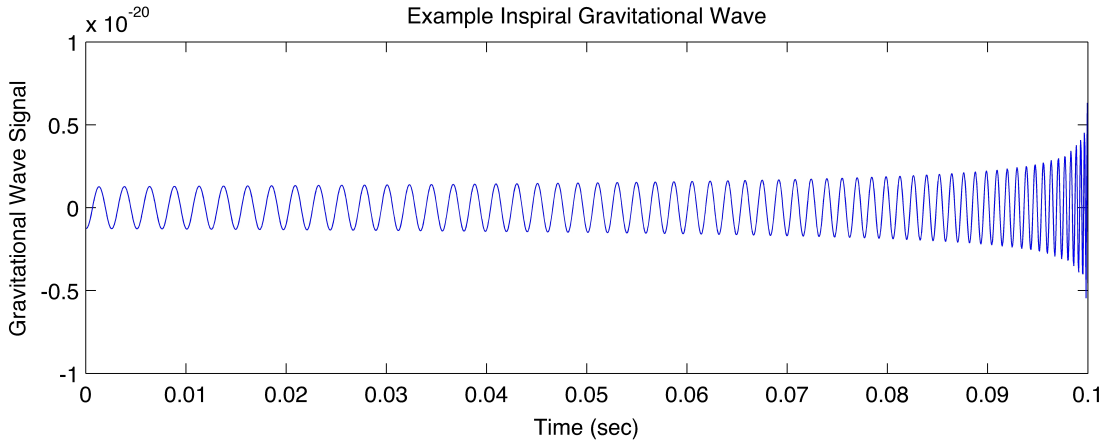

Figure 3.2: Inspiral signal from binary system.[1]

[1] http://www.ligo.org/science/GW-Overview/images/inspiral.jpg

3.5 Binary black hole mergers in the early advanced LIGO-Virgo era

Exactly a hundred years after the prediction of gravitational waves by Einstein's theory of general relativity [16], the first observation has been announced by the LIGO-Virgo collaboration in 2016 [11], and so far there are three confirmed observations, all coming from BH-BH merger.

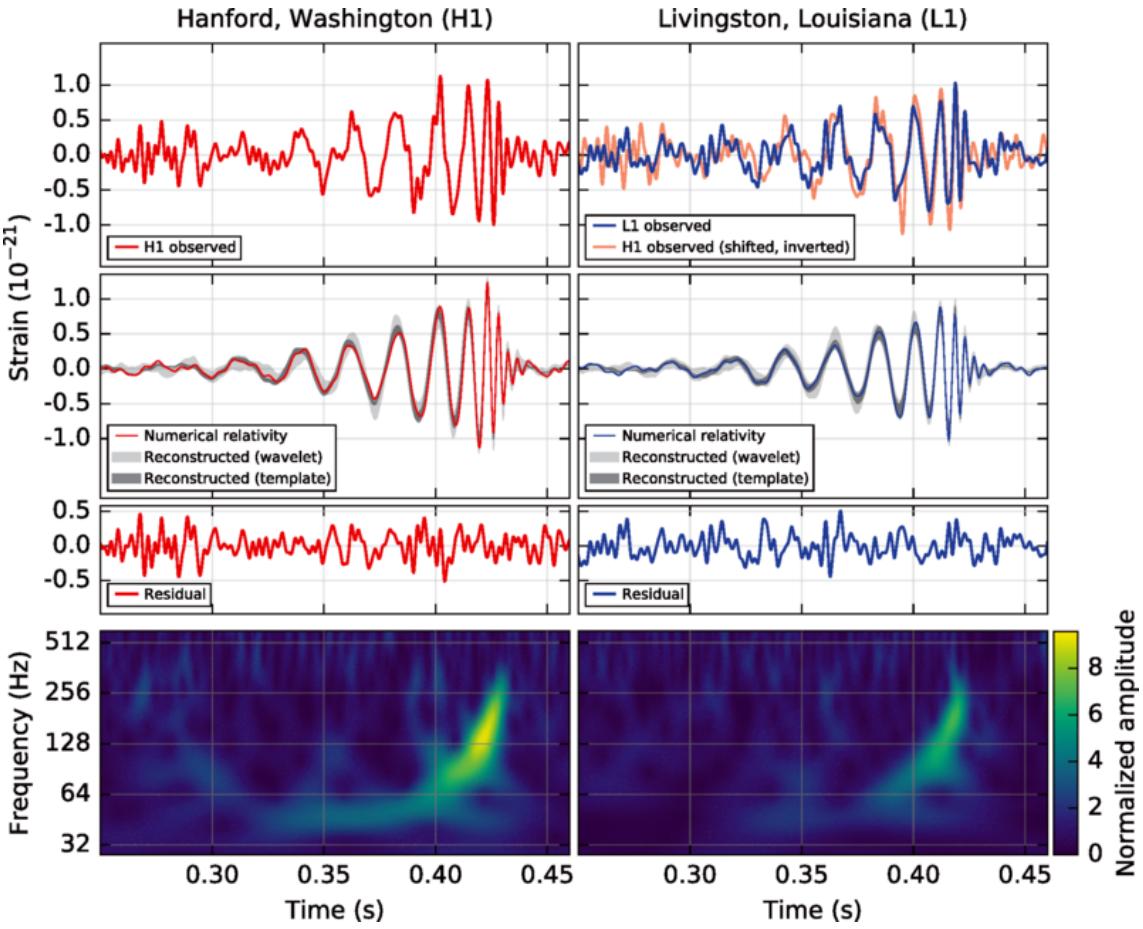

Figure 3.3: The first gravitational wave event observed by LIGO detectors. [11]

In Figure 3.3 we show the signal detected on September 14, 2015, at 09:50:45 UTC, by the LIGO Hanford, WA, and Livingston, LA, observatories, later confirmed in 2016. In the top charts we see the signal detected by the two interferometers, H1 data being shifted in time because the signal arrived first at L1. Unlike the other two events, we can clearly see the inspiral and the ringdown waveform, because of the very high signal-to-noise ratio of the mergers. In the second row we see the

reconstructed signal: in particular the thin line in red (blue) on the left (right) chart represents the numerical relativity predicted waveform. In the third row there are the residual after subtracting the numerical relativity waveform from the detected signal. Finally, in the last row we have a time-frequency plot of the strain data, showing the signal frequency increasing in time together with the amplitude, according to our calculations in the previous sections. In Table 3.1 we show the

Event	$m_1/M_\odot$	$m_2/M_\odot$	$M_f/M_\odot$	D_L Mpc
GW150914	$35.4^{+5.0}_{-3.4}$	$29.8^{+3.3}_{-4.3}$	$62.2^{+3.7}_{-3.4}$	440^{+160}_{-180}
GW151226	$14.2^{+8.3}_{-3.7}$	$7.5^{+2.3}_{-2.3}$	$20.8^{+6.1}_{-1.7}$	440^{+180}_{-190}
GW170104	$31.2^{+8.4}_{-6.0}$	$19.4^{+5.3}_{-5.9}$	$48.7^{+5.7}_{-4.6}$	880^{+450}_{-390}

Table 3.1: Current observations of binary black hole systems.

current data for present observations [17, 18, 19]. Together with the name of the event, we report the mass m_1 and m_2 of the two object, the final mass M_f after the merger and the luminosity distance D_L. The latter is known with a big uncertainty because we cannot determine the relative orientation of the system to the sight line, due to the inability of the current network of detectors to discern both polarizations of the GW signal. In Figure 3.4 we report the current prediction by the LIGO-Virgo

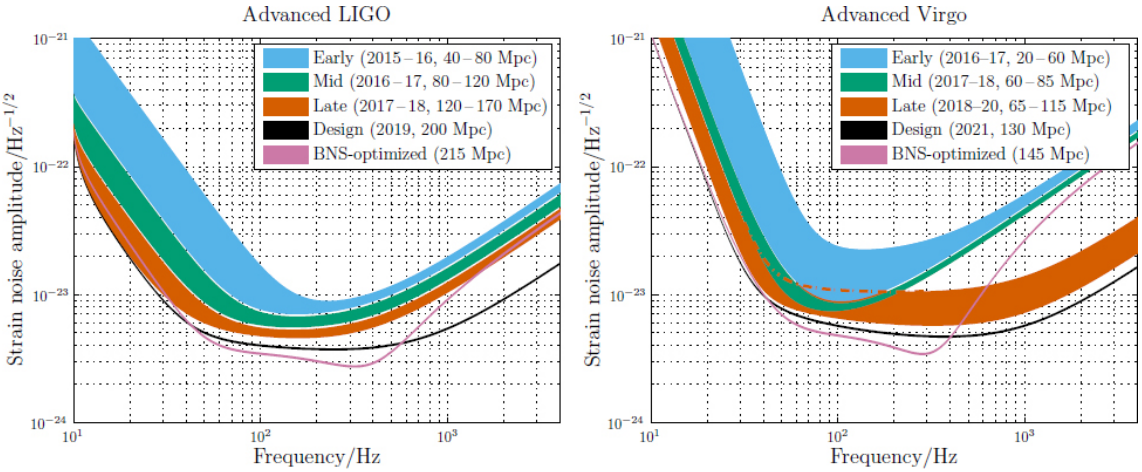

Figure 3.4: Advanced LIGO (left) and advanced Virgo (right) target strain sensitivity as a function of frequency. [20]

collaboration about the future sensitivity that will be reached by the detectors.

A binary NS merger detection is highly awaited as the next most important breakthrough. Besides being a very promising source of GWs, these events offer a unique opportunity to constrain the NS EOS. Moreover, they are likely accompanied

by a rich variety of electromagnetic signals, the most relevant of which will be discussed in the next chapter.

4 Electromagnetic radiation from binary neutron star systems

As we already pointed out previously, BH-BH mergers are not expected to produce bright electromagnetic (EM) signals. Conversely, mergers involving NSs are expected to link EM and GW skies. EM signals generated from NS-BH and binary NS (BNS) systems cover the entire EM spectrum and they are emitted over a variety of timescales. There are several reasons to study these signals. For example, by detecting the EM counterpart to the GW will give an opportunity to identify the host galaxy and the relative position of the source to it: this will provide valuable information on binary formation channels, age of the stellar population and supernova birth kicks. In addition, this identification can allow us to determine the redshift and thus estimate the distance of the source, which is typically measured with very high uncertainty from a GW detection alone (as seen in Table 3.1). Moreover, a combined EM and GW observation can prove the connection between short gamma-ray bursts (SGRBs) and binary NS or NS-BH mergers, revealing information on when and how they can be produced. Finally, EM signal alone can reveal exclusive information on the physics of the merger and post-merger phases, especially if the remnant is a massive NS.

In the following, we give a brief overview of the most promising EM signals expected in association with BNS mergers.

4.1 Short gamma-ray bursts

SGRBs are the brightest events known in the Universe. They consist in highly energetic photon beams (observable in the gamma-ray band) that light up a tiny region in the sky for less than $\sim 2\,\mathrm{s}$. SGRBs are among the earliest proposed counterparts to the GW signal form BNS and NS-BH mergers. The leading (standard) model explains this emission via a relativistic outflow (jet) generated by a torus of matter accreting onto a remnant BH, that is formed soon ($< 10 - 100\,\mathrm{ms}$) after the merger [21, 22, 23, 24, 25, 26]. However, the physical mechanism that would launch the jet is still uncertain. Two commonly invoked mechanisms are the neutrino and the magnetic mechanism:

- neutrinos and antineutrinos copiously emitted by the accretion disk deposit thermal energy at the poles of the BH via annihilation. The produced e^+/e^- are accelerated to relativistic velocities and decelerated by the external matter (interstellar medium or previously ejected matter), and shocks within different

waves generate the gamma-ray burst [27].

- strong poloidal magnetic field threading the BH can remove angular momentum from the BH itself via the Blandford–Znajek process [28]. If the magnetic field is strong enough a cascade pair production which can power the jet is generated.

Recent simulations indicate that the neutrino mechanism seems to be too weak to drive a powerful enough jet. Hence, the energy requirements favour magnetic fields as the main driving force. Since magnetic fields are likely to play a key role in the formation of a jet, we need general relativistic magnetohydrodynamic simulations to investigate the nature of these events. In Figure 4.1 we show a recent BNS merger simulation where an "incipient jet" starts to emerge after the BH has formed [29].

The above standard BH-disk paradigm, however, leaves important open questions. According to the model, the energy release should stop once the torus has been accreted on a timescale of $< 1\,\mathrm{s}$, which is consistent with SGRBs timescales. Nevertheless, recent observations by the Swift satellite [30] revealed long-lasting ($\sim 10^2 - 10^5\,\mathrm{s}$) X-ray afterglows in a large fraction of SGRB events, which are difficult to explain by the short accretion timescale of the torus. These afterglows could be explained in a different scenario in which the BNS merger result in a stable or long-lived NS rather than a BH, with the additional energy release powered by the loss of rotational energy via magnetic spindown [31, 32, 33]. This so-called "magnetar" model has its own difficulties. In particular, the much higher baryon pollution expected in this case in the surrounding of the merger site makes it more difficult to launch a jet, which might not be able to pierce through a denser environment.

A third alternative is offered by the recently proposed "time-reversal" scenario [34], which overcomes the problems of the BH-disk and magnetar scenarios. The jet engine of this model is a long-lived supramassive NS produced by a BNS merger, which eventually collapses to a BH on timescales of $\sim$ minutes or even longer. The magnetized NS remnant injects energy to the surrounding matter via EM spindown (see Section 4.3). Then it collapses to a BH and creates the conditions to generate a jet. The merger site is then surrounded by a plasma nebula inflated by the EM spindown and by an external layer of isotropic baryon-loaded ejecta expelled in the post-merger phase, which is now at lower densities. While the jet easily drills through the environment and produce the gamma-ray emission, the spindown energy is trapped inside the nebula and diffuses on much longer timescales. As a result, the spindown-powered X-ray emission can still be observed for a long time after the SGRB itself, explaining in this way the long-lasting X-ray afterglows. This scenario can thus explain both the SGRB and the X-ray afterglows. Nevertheless, it cannot be validated by present simulations since it covers timescales that are now inaccessible.

If any of these scenarios is correct, observing a SGRB in coincidence with the GW signal from a compact binary coalescence would represent a "smoking-gun" confirmation of the association between these events and mergers involving a NS.

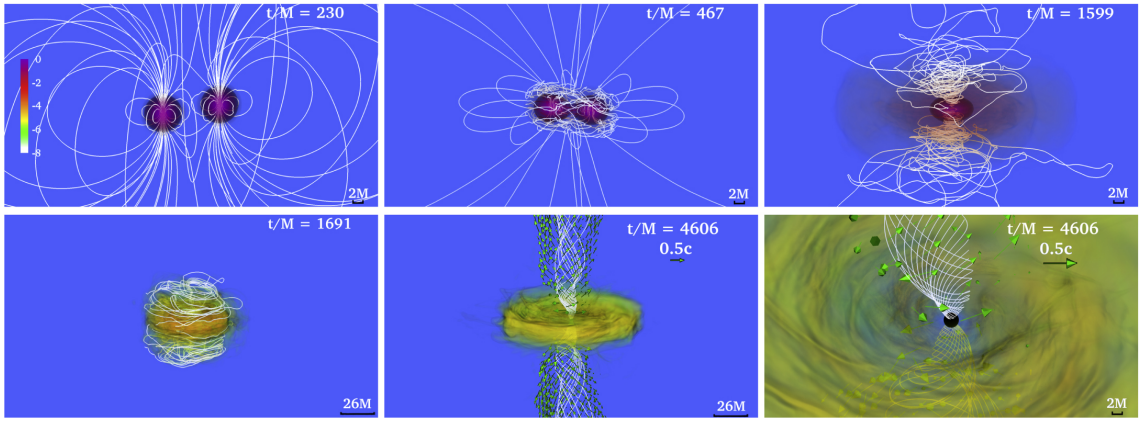

Figure 4.1: Simulation of a BNS merger with SGRB generation. The arrows indicate plasma velocities, and the white lines show the B-field structure. [29]

4.2 Kilonova/Macronova transients

Kilonovae or macronovae are another important EM counterpart to the GW signal for BNS mergers and NS-BH mergers (e.g., [35] and refs. therein). This radiation is emitted at optical and infrared wavelengths, with timescales of days to weeks. It is powered by the heating generated from radioactive decay of r-process elements, produced in the sub-relativistic ejecta. The merger ejects a small fraction of matter at sub-relativistic velocity; since NS is primary composed by neutron-rich nuclei and free neutrons, r-process nucleosynthesis is expected to take place. Free neutrons impact on heavy (^{56}Fe or heavier) nuclei creating unstable isotopes via rapid neutron capture, which can undergo β-decay. Radioactivity provides a long-term heat source for the expanding envelope, and heavy elements filter out the high energy radiation, allowing only the lower energy signal to escape.

A simultaneous detection of kilonova/macronova and a GW signal would provides rich information about the merger events. It can be useful for determining the host galaxy of the source and since its lightcurve reflects the binary parameters, it could also be useful for extracting the physical information of the binary.

4.3 Spin-down powered transients from long-lived NS remnants

As discussed at the end of Chapter 2, BNS mergers can produce a long-lived massive NS remnant. This has important consequences. First, neutrinos and magnetically driven outflows can provide an additional source of ejecta material for the r-process nucleosynthesis. Second, the magnetized NS remnant emits EM spin-down radiation, and this can power a nearly isotropic transient when reprocessed through the surrounding pulsar wind and the matter ejected during the merger (e.g. [36, 37]). This emission represents a potentially promising counterpart to the GW signal from BNS mergers (while it is absent for NS-BH mergers) and provides a possible explanation for the long-lasting X-ray afterglows of SGRBs (see Section 4.1). Since spin-down radiation is exclusive of long-lived NS remnants, detecting this signal would be an evidence that the product of the BNS merger is a long-lived NS.

5 Conclusions

The Theory of general relativity has been one of the biggest revolutions in physics and in our way to conceive the Universe, eradicating the concepts of absolute space and time postulated by the classical mechanics. About a hundred years ago Albert Einstein predicted that, as a stone falling on the smooth surface of a lake would generate small ripples on it, a perturbation of the smooth space-time metric would also generate ripples in the shape of space-time itself. For exactly a hundred years, gravitational waves remained a prediction, until 2016. With the first observation of a gravitational wave by the LIGO interferometer, a new era of physics has begun: we have now a new sense to probe the Universe. With the capability to detect gravitational waves we can gain complementary information to those obtained by electromagnetic spectrum detectors, and we can study objects which were invisible before, like black holes.

Binary neutron star mergers represent the ultimate targets for a multi-messenger astrophysics. As we have seen, they are the most promising source of both electromagnetic and gravitational signals. The extreme conditions in which neutron stars form and live, and the catastrophic events in the merger and post-merger phases provide a rich phenomenology and a unique opportunity to test theories in conditions not reproducible on Earth.

In Chapter 3 we formally derived the equations for a gravitational wave propagating in space-time, starting from the linearized field equations of general relativity, and below we solved analytically the case of two objects in circular orbit around the system's centre of mass, and we found the waveform for the inspiral phase. However, as we pointed out, this is an approximation, which is valid only when the objects are far enough so that the weak field and the slow motion conditions hold on. In fact, the spherical symmetry of the neutron star is an approximation too. While there is a chance to solve analytically the inspiralling system, no chances are given for the merger phase. When the stars start to be close enough that the weak field approximation doesn't hold on anymore, we cannot apply the linearized field equations. Thus, we need full general relativistic simulations to compute the signal expected. In addition, since neutron star magnetic fields are very strong, magnetohydrodynamics comes into play and makes things more complicated.

In Chapter 4 we have briefly shown the most promising electromagnetic counterparts to the gravitational wave signal for a binary neutron star merger. Unlike Chapter 3, we have not given a mathematical background for these signals. As we discussed, there is not a generally accepted model to explain those type of emissions, in particular for the short gamma-ray bursts, and most of the information we have comes from simulations.

To conclude, although there is still much to understand, new research scenarios have now become reality thanks to the LIGO-Virgo collaboration, enabling us to deeply investigate the physics and astrophysics of binary neutron star mergers.

Bibliography

[1] W. Baade and F. Zwicky. "On Super-novae". In: *Proceedings of the National Academy of Science* 20 (May 1934), pp. 254–259. DOI: 10.1073/pnas.20.5.254.

[2] J. Chadwick. "Possible Existence of a Neutron". In: *Nature* 129 (Feb. 1932), p. 312. DOI: 10.1038/129312a0.

[3] A. Hewish et al. "Observation of a Rapidly Pulsating Radio Source". In: *Nature* 217 (Feb. 1968), pp. 709–713. DOI: 10.1038/217709a0.

[4] T. Gold. "Rotating Neutron Stars as the Origin of the Pulsating Radio Sources". In: *Nature* 218 (May 1968), pp. 731–732. DOI: 10.1038/218731a0.

[5] F. Pacini. "Rotating Neutron Stars, Pulsars and Supernova Remnants". In: *Nature* 219 (July 1968), pp. 145–146. DOI: 10.1038/219145a0.

[6] S. L. Shapiro and S. A. Teukolsky. *Black Holes, White Dwarfs and Neutron Stars: The Physics of Compact Objects*. June 1986, p. 672.

[7] J. M. Lattimer and M. Prakash. "Neutron star observations: Prognosis for equation of state constraints". In: *Physics Reports* 442 (Apr. 2007), pp. 109–165. DOI: 10.1016/j.physrep.2007.02.003. eprint: astro-ph/0612440.

[8] D. R. Lorimer. "Binary and Millisecond Pulsars". In: *Living Reviews in Relativity* 11 (Nov. 2008). DOI: 10.12942/lrr-2008-8. arXiv: 0811.0762.

[9] P. B. Demorest et al. "A two-solar-mass neutron star measured using Shapiro delay". In: *Nature* 467 (Oct. 2010), pp. 1081–1083. DOI: 10.1038/nature09466. arXiv: 1010.5788 [astro-ph.HE].

[10] J. Antoniadis et al. "A Massive Pulsar in a Compact Relativistic Binary". In: *Science* 340 (Apr. 2013), p. 448. DOI: 10.1126/science.1233232. arXiv: 1304.6875 [astro-ph.HE].

[11] B. P. Abbott et al. "Observation of Gravitational Waves from a Binary Black Hole Merger". In: *Phys. Rev. Lett.* 116 (6 Feb. 2016), p. 061102. DOI: 10.1103/PhysRevLett.116.061102. URL: https://link.aps.org/doi/10.1103/PhysRevLett.116.061102.

[12] L. Baiotti and L. Rezzolla. "Binary neutron-star mergers: a review of Einstein's richest laboratory". In: *ArXiv e-prints* (July 2016). arXiv: 1607.03540 [gr-qc].

[13] R. Ciolfi et al. "General relativistic magnetohydrodynamic simulations of binary neutron star mergers forming a long-lived neutron star". In: *Physical Review D* 95.6, 063016 (Mar. 2017), p. 063016. DOI: 10.1103/PhysRevD.95.063016. arXiv: 1701.08738 [astro-ph.HE].

[14] A. Endrizzi et al. "General relativistic magnetohydrodynamic simulations of binary neutron star mergers with the APR4 equation of state". In: *Classical and Quantum Gravity* 33.16, 164001 (Aug. 2016), p. 164001. DOI: 10.1088/0264-9381/33/16/164001. arXiv: 1604.03445 [astro-ph.HE].

[15] W. Kastaun and F. Galeazzi. "Properties of hypermassive neutron stars formed in mergers of spinning binaries". In: *Physical Review D* 91.6, 064027 (Mar. 2015), p. 064027. DOI: 10.1103/PhysRevD.91.064027. arXiv: 1411.7975 [gr-qc].

[16] A. Einstein. "Näherungsweise Integration der Feldgleichungen der Gravitation". In: *Sitzungsberichte der Königlich Preußischen Akademie der Wissenschaften (Berlin), Seite 688-696.* (1916).

[17] B. P. Abbott et al. "Improved Analysis of GW150914 Using a Fully Spin-Precessing Waveform Model". In: *Physical Review X* 6.4, 041014 (Oct. 2016), p. 041014. DOI: 10.1103/PhysRevX.6.041014. arXiv: 1606.01210 [gr-qc].

[18] B. P. Abbott et al. "GW151226: Observation of Gravitational Waves from a 22-Solar-Mass Binary Black Hole Coalescence". In: *Phys. Rev. Lett.* 116 (24 June 2016), p. 241103. DOI: 10.1103/PhysRevLett.116.241103. URL: https://link.aps.org/doi/10.1103/PhysRevLett.116.241103.

[19] B. P. Abbott et al. "GW170104: Observation of a 50-Solar-Mass Binary Black Hole Coalescence at Redshift 0.2". In: *Phys. Rev. Lett.* 118 (22 June 2017), p. 221101. DOI: 10.1103/PhysRevLett.118.221101. URL: https://link.aps.org/doi/10.1103/PhysRevLett.118.221101.

[20] B. P. Abbott et al. "Prospects for Observing and Localizing Gravitational-Wave Transients with Advanced LIGO and Advanced Virgo". In: *Living Reviews in Relativity* 19, 1 (Feb. 2016), p. 1. DOI: 10.1007/lrr-2016-1. arXiv: 1304.0670 [gr-qc].

[21] B. Paczynski. "Gamma-ray bursters at cosmological distances". In: *The Astrophysical Journal Letters* 308 (Sept. 1986), pp. L43–L46. DOI: 10.1086/184740.

[22] D. Eichler et al. "Nucleosynthesis, neutrino bursts and gamma-rays from coalescing neutron stars". In: *Nature* 340 (July 1989), pp. 126–128. DOI: 10.1038/340126a0.

[23] R. Narayan, B. Paczynski, and T. Piran. "Gamma-ray bursts as the death throes of massive binary stars". In: *The Astrophysical Journal Letters* 395 (Aug. 1992), pp. L83–L86. DOI: 10.1086/186493. eprint: astro-ph/9204001.

[24] D. B. Fox et al. "The afterglow of GRB 050709 and the nature of the short-hard γ-ray bursts". In: *Nature* 437 (Oct. 2005), pp. 845–850. DOI: 10.1038/nature04189. eprint: astro-ph/0510110.

[25] N. Gehrels et al. "A short γ-ray burst apparently associated with an elliptical galaxy at redshift z = 0.225". In: *Nature* 437 (Oct. 2005), pp. 851–854. DOI: 10.1038/nature04142. eprint: astro-ph/0505630.

[26] S. D. Barthelmy et al. "An origin for short γ-ray bursts unassociated with current star formation". In: *Nature* 438 (Dec. 2005), pp. 994–996. DOI: 10.1038/nature04392. eprint: astro-ph/0511579.

[27] P. Mészáros. "Photospheres, Comptonization and X-ray lines in gamma-ray bursts". In: *Gamma-ray Bursts, 5th Huntsville Symposium*. Ed. by R. M. Kippen, R. S. Mallozzi, and G. J. Fishman. Vol. 526. American Institute of Physics Conference Series. Sept. 2000, pp. 514–518. DOI: 10.1063/1.1361591. eprint: astro-ph/9912474.

[28] R. D. Blandford and R. L. Znajek. "Electromagnetic extraction of energy from Kerr black holes". In: *Monthly Notices of the Royal Astronomical Society* 179 (May 1977), pp. 433–456. DOI: 10.1093/mnras/179.3.433.

[29] M. Ruiz et al. "Binary Neutron Star Mergers: A Jet Engine for Short Gamma-Ray Bursts". In: *The Astrophysical Journal Letters* 824, L6 (June 2016), p. L6. DOI: 10.3847/2041-8205/824/1/L6. arXiv: 1604.02455 [astro-ph.HE].

[30] N. Gehrels et al. "The Swift Gamma-Ray Burst Mission". In: *The Astrophysical Journal* 611.2 (2004), p. 1005. URL: http://stacks.iop.org/0004-637X/611/i=2/a=1005.

[31] Bing Zhang and Peter Mészáros. "Gamma-Ray Burst Afterglow with Continuous Energy Injection: Signature of a Highly Magnetized Millisecond Pulsar". In: *The Astrophysical Journal Letters* 552.1 (2001), p. L35. URL: http://stacks.iop.org/1538-4357/552/i=1/a=L35.

[32] Wei-Hong Gao and Yi-Zhong Fan. "Short-living Supermassive Magnetar Model for the Early X-ray Flares Following Short GRBs". In: *Chinese Journal of Astronomy and Astrophysics* 6.5 (2006), p. 513. URL: http://stacks.iop.org/1009-9271/6/i=5/a=01.

[33] B. D. Metzger, E. Quataert, and T. A. Thompson. “Short-duration gamma-ray bursts with extended emission from protomagnetar spin-down”. In: *Monthly Notices of the Royal Astronomical Society* 385.3 (2008), pp. 1455–1460. DOI: 10.1111/j.1365-2966.2008.12923.x. eprint: /oup/backfile/content_public/journal/mnras/385/3/10.1111/j.1365-2966.2008.12923.x/2/mnras0385-1455.pdf. URL: +%20http://dx.doi.org/10.1111/j.1365-2966.2008.12923.x.

[34] Riccardo Ciolfi and Daniel M. Siegel. “Short Gamma-Ray Bursts in the "Time-reversal" Scenario”. In: *The Astrophysical Journal Letters* 798.2 (2015), p. L36. URL: http://stacks.iop.org/2041-8205/798/i=2/a=L36.

[35] B. D. Metzger. “Kilonovae”. In: *Living Reviews in Relativity* 20, 3 (May 2017), p. 3. DOI: 10.1007/s41114-017-0006-z. arXiv: 1610.09381 [astro-ph.HE].

[36] D. M. Siegel and R. Ciolfi. “Electromagnetic Emission from Long-lived Binary Neutron Star Merger Remnants. II. Lightcurves and Spectra”. In: *The Astrophysical Journal* 819, 15 (Mar. 2016), p. 15. DOI: 10.3847/0004-637X/819/1/15. arXiv: 1508.07939 [astro-ph.HE].

[37] D. M. Siegel and R. Ciolfi. “Electromagnetic Emission from Long-lived Binary Neutron Star Merger Remnants. I. Formulation of the Problem”. In: *The Astrophysical Journal* 819, 14 (Mar. 2016), p. 14. DOI: 10.3847/0004-637X/819/1/14. arXiv: 1508.07911 [astro-ph.HE].